Astron. Astrophys. 353, 1065–1073 (2000)

ASTRONOMY AND ASTROPHYSICS

The distribution of OH in Taurus Molecular Cloud-1

J. Harju[1], **A. Winnberg**[2], **and J.G.A. Wouterloot**[3]

[1] Observatory, P.O. Box 14, University of Helsinki, 00014 Helsinki, Finland
[2] Onsala Space Observatory, 43992 Onsala, Sweden
[3] Radioastronomisches Institut, Universität Bonn, Auf dem Hügel 71, 53121 Bonn, Germany

Received 26 April 1999 / Accepted 9 November 1999

Abstract. The column density of the OH radical in Taurus Molecular Cloud-1 (TMC-1), reaches its maximum close to the cyanopolyyne peak. A comparison with previously published maps of other molecules shows that OH has a similar distribution as HC_3N and CCS, but differs largely from CS, SO, NH_3 and N_2H^+. The OH/$C^{18}O$ column density ratio is, however, almost constant along the dense ridge of TMC-1, suggesting that the fractional OH abundance does not change much, the derived value being about 10^{-7}. This high number confirms that in dense gas OH is mainly formed by the electron recombination of H_3O^+. The approximate constancy of the fractional OH abundance is in accordance with a flat density distribution as has been derived recently (Pratap et al. 1997).

Previous SO/CS maps together with some recent modelling results seem to be in conflict with the idea that the cyanopolyyne peak in the southeastern part of the cloud would be chemically less evolved than the ammonia maximum in the northwest. Therefore we discuss the possibility that the OH maximum represents the so called 'radical peak', which occurs when freezing on to grain surfaces starts to be the dominant factor controlling the chemical composition and reactions (Brown & Millar 1989). It turns out that the greater part of the data accumulated so far, including the present OH observations, fit the 'old' picture where a slightly higher density and a more advanced chemical state prevail in the northwestern part of the TMC-1 ridge.

The 'satellite' lines towards two locations in the cloud show enhanced 1612 MHz emission. We suggest that this is due to non-thermal excitation by far-infrared radiation from dust, heated by the embedded young stars in the neighbourhood of the TMC-1 ridge.

Key words: molecular processes – ISM: abundances – ISM: clouds – ISM: molecules – ISM: individual objects: TMC-1

1. Introduction

The OH radical is linked with the production of H_2O and O_2 in molecular clouds. In cold gas OH is formed together with H_2O by dissociative recombination of H_3O^+ with electrons. The chain of reactions leading to H_3O^+ is initiated by the proton transfer reaction

$$O + H_3^+ \longrightarrow OH^+ + H_2 \quad (1)$$

(see e.g. Viala 1986; Hartquist & Williams 1995). The OH^+ ion then reacts with H_2 to form H_2O^+ which again can deprive another H_2 of an H atom. According to the recent measurements by Vejby-Christensen et al. (1997) OH and H_2O should be produced in the electron recombination with probabilities of 66 and 33 percent, respectively, the remaining one percent being for the creation of O + H + H. The ground-state transition of H_2O at 557 GHz requires a very high density to be collisionally excited, making the detection difficult towards dark clouds (see Phillips & Green 1995 and references therein).

The formation of O_2 occurs in the gas phase via the neutral exchange reaction between O and OH, which is also the main sink for OH in dense regions:

$$OH + O \longrightarrow O_2 + H\ . \quad (2)$$

Note that atomic oxygen takes part both in the production and destruction of OH and thus the abundance of OH depends mainly on the H_3^+ abundance and accordingly on the ionization rate of H_2. Molecular oxygen is destroyed by carbon atoms according to

$$C + O_2 \longrightarrow CO + O \quad (3)$$

(see e.g. Millar & Nejad 1985). Assuming that reactions (2) and (3) dominate the O_2 chemistry, regions with high O and OH abundances and a low C abundance look particularly favourable for searches in the interstellar medium for the so far undetected O_2.

Taurus Molecular Cloud 1 (TMC-1, Churchwell et al. 1979) is known for its chemical gradient with distinct C_4H, HC_7N and NH_3 maxima (Little et al. 1979; Olano et al. 1988). The elongated core is fragmented into at least five clumps (Hirahara et al. 1992; Langer et al. 1995). The northernmost of these clumps has an infrared source in its vicinity (IRAS 04381+2540). The existence of complex carbon compounds towards the cyanopolyyne maximum in the southeastern part of TMC-1 has been explained by a relatively high abundance of carbon atoms, either due to an early stage of chemical evolution or to an exceptionally high atomic C/O abundance ratio (Herbst 1983; Millar & Nejad 1985; Herbst & Leung 1989;

Send offprint requests to: J. Harju (jorma.harju@astro.helsinki.fi)

Hartquist et al. 1996). In the northwestern part, where for example the NH_3, SO, HCO^+ and N_2H^+ maxima lie (Guélin et al. 1982; Hirahara et al. 1995; Pratap et al. 1997), C is supposed to be processed to CO.

According to time-dependent gas-phase chemistry models (e.g. Millar & Nejad 1985, Millar et al. 1997), the variation in the abundance of O is clearly less marked than for C. The suggested variation in the O/C abundance ratio along the TMC-1 ridge should be reflected in the O_2 distribution, provided that it is not compensated by an opposite gradient in the abundance of OH.

The purpose of the present study is to determine the distribution of OH in TMC-1, and thereby provide useful data to the interpretation of the SWAS and Odin satellite observations. Both satellites will try to detect lines of O_2 and H_2O towards this object. The only transition of OH excited in conditions typical of dark clouds is the ground electronic state Λ-doublet line with 4 hyperfine components at $\lambda = 18$ cm. Although the angular resolution of the present observations is modest ($\sim 8'$), it matches well the resolution of the Odin 1.1-m antenna at 119 GHz (the frequency of the magnetic dipole transition $N_J = 1_1 \rightarrow 1_0$ of O_2). Accordingly, a direct comparison of OH and O_2 will be possible. Comparison between the 2.5-mm O_2 and 18-cm OH lines is furthermore facilitated by the fact they are both thermalized already at densities of about 10^4 cm^{-3} (Guibert et al. 1978; Bergman 1995; Maréchal et al. 1997).

The plan of this paper is as follows: In Sect. 2 we describe the observations. In Sect. 3 the results from the observations are presented and these are further discussed in Sect. 4. In Sect. 5 we summarize our conclusions.

2. Observations

The observations were made during two runs, in December 1996 and in December 1997, with the 100-m telescope of Max-Planck-Institut für Radioastronomie, Bonn, situated near Effelsberg, Germany. The 'main' Λ-doublet hyperfine lines of OH at 1667 and 1665 MHz were observed simultaneously in the LHC and RHC polarizations, by utilizing the dual channel 1.7 GHz receiver and the possibility of choosing the centre frequencies of the four IF channels of the 1024 channel autocorrelator individually. The total bandwidth of the spectrometer was set to 781.25 kHz. The resulting spectrometer channel width is 760 Hz corresponding to 0.14 kms^{-1}. The observations were made in the frequency switching mode with a throw corresponding to 64 channels (about 50 kHz).

The beam-width of the telescope at 1.7 GHz is $7\farcm8$, and the aperture and main-beam efficiencies at this frequency are 0.49 and 0.70, respectively. The system temperatures with the 1.7 GHz receiver were 42 and 50 K for the A (LHC) and B (RHC) channels, respectively, in the antenna temperature scale. The typical integration time was 12 minutes (total time for both phases together), which yielded, after 'folding' and averaging the two polarizations an RMS noise level of 0.08 K in the main beam brightness temperature, $T_{\rm MB}$, scale.

The calibration was achieved by observing the standard continuum calibration sources 3C123 and 3C48. The flux densities at the frequencies 1612, 1666 and 1720 MHz were adopted from the updated list of Ott et al. (1994). The intensity scale of the spectra were converted to the $T_{\rm MB}$ scale by using the averages of the $T_{\rm MB}$/calibration units ratio for the two receiver channels (A and B) obtained from the standard calibrators.

The ridge of TMC-1 was mapped in the 'main lines' over 83 positions with a spacing of $4'$ ($\sim 1/2$ HPBW). The map was centered on the $C^{18}O$ maximum as observed by Langer et al. (1995; $\alpha_{1950.0} = 4^h38^m8\fs7, \delta_{1950.0} = 25^\circ44'20''$), and it was tilted by $54\fdg5$ with respect to the declination axis in order to cover the molecular ridge by a regular grid of observing points.

The 'satellites' at 1612 and 1720 MHz were observed towards three locations at the offsets $(0', 0')$, $(7\farcm0, -9\farcm8)$ and $(-11\farcm2, 1\farcm9)$ from the map centre. These lines were observed separately but in the LHC and RHC polarizations simultaneously. The satellites were detected only towards $(0', 0')$ and $(7\farcm0, -9\farcm8)$. The spectra of all four hyperfine components towards these two locations are shown in Fig. 1.

3. Results

3.1. Integrated intensity and channel maps

The integrated intensity maps of the 'main lines' of OH at 1667 and 1665 MHz are shown in Fig. 2. Emission is detected in the velocity range $4.6 - 7.1$ kms^{-1}, but we have plotted the integrated intensity between 5 and 7 kms^{-1} to enable a direct comparison with the $C^{18}O$ map of Langer et al. (1995). The map of the full range and the one presented are, however, practically identical. The lines are detected everywhere in the mapped region which has a size of about $40'$ by $30'$. Despite the large beam size the dense ridge of TMC-1 can be well discerned in the map. The 1667 MHz OH emission clearly peaks towards the cyanopolyyne and C_4H maxima in the southeast. This peaking is less prominent in the 1665 MHz line. The locations of those IRAS point sources, which probably are associated with the cloud and lie within or just outside the mapped region are indicated in Fig. 2. The numbers refer to Table 3 of Onishi et al. (1998). The significance of the embedded infrared sources is discussed in Sect. 4.

The OH lines are generally divided into two main components separated by a dip occurring almost constantly at the LSR velocity 5.8 kms^{-1} (see Fig. 1). Previous high-resolution studies in other molecules (Hirahara et al. 1992; Langer et al. 1995; Pratap et al. 1997) have, however, revealed a complex spatial-velocity distribution. In order to compare the OH distribution with the results of these previous studies we present in Figs. 3 and 4 velocity channel maps for the 1667 and 1665 MHz lines between 5.0 and 6.6 kms^{-1}, using a channel separation of 0.4 kms^{-1}. The 1665 MHz line is probably optically thin (see below) and thus gives a more penetrating view of the cloud structure.

It can be seen from the channel maps that emission in the lowest velocity range ($5.0 - 5.4$ kms^{-1}) comes from a separate core which is located about $15'$ north of our nominal centre, and

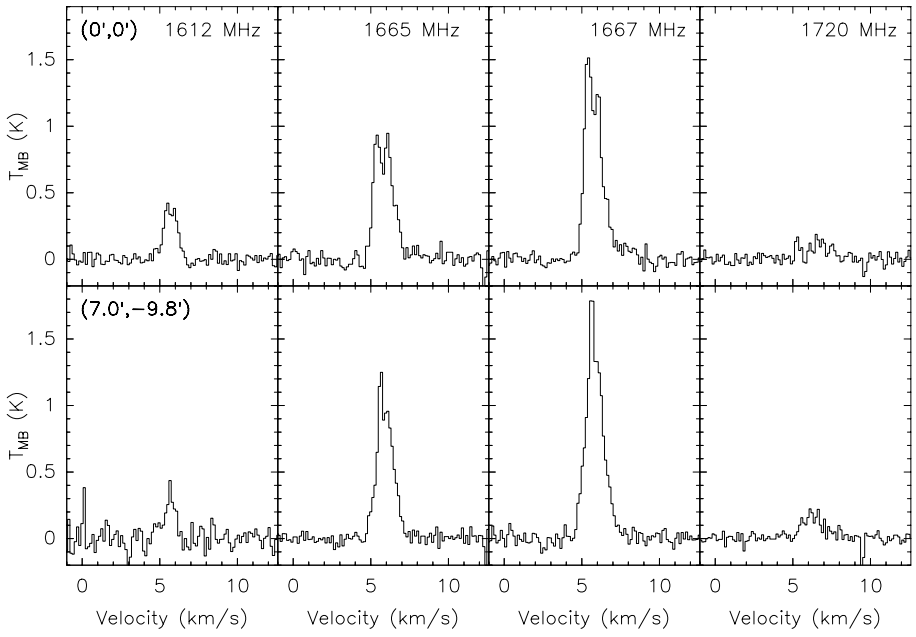

Fig. 1. The four hyperfine components of the Λ-doubling line of OH in the ground rotational level towards two locations in the TMC-1 ridge. The $(0', 0')$ position corresponds to the $C^{18}O$ emission maximum (Langer et al. 1995) and the offset $(7'.0, -9'.8)$ is located $12'$ to the southeast from the latter, close to the cyanopolyyne maximum. The optically thin LTE ratios of the lines from left to right are $0.19 : 1.00 : 1.80 : 0.21$. This implies that in LTE the 1612 MHz and 1720 MHz lines should be equally strong.

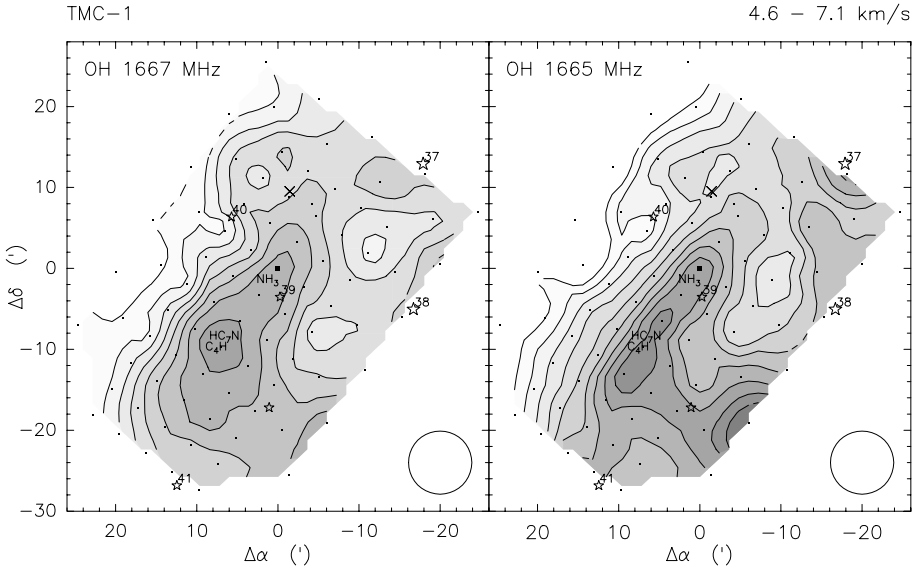

Fig. 2. Integrated intensity maps of the OH 1667 MHz and 1665 MHz lines in the velocity range $5 - 7$ kms^{-1}. The lowest contour is 0.6 K kms^{-1} and the increments are 0.2 and 0.1 K kms^{-1} for the 1667 MHz and 1665 MHz lines, respectively. The $(0, 0)$ position, $\alpha_{1950.0} = 4^h38^m8^s.7, \delta_{1950.0} = 25°44'20''$, is marked by a small filled square. The locations of the IRAS point sources within or near the edge of the mapped region (Onishi et al. 1998) and the locations of the NH_3, HC_7N and C_4H emission maxima (Olano et al. 1988) are indicated. The cross in the north indicates the location IRAS 04380+2553 and the unlabelled source in the south is IRAS 04383+2527.

from the northwestern part of the TMC-1 ridge, around the Hirahara clumps A and B. The northern core belongs to the region called Heiles Cloud 2-C or TMC-1C (Cernicharo et al. 1984; Cernicharo & Guélin 1987; Takakuwa et al. 1998). The distribution in the next velocity channel ($5.4-5.8$ kms^{-1}) is markedly different from the previous one, being concentrated on the southeastern clumps D and E. In the range $5.8 - 6.2$ kms^{-1} the maximum moves further towards southeast beyond the C_4H peak discovered by Olano et al. (1988). The dense ridge can be outlined in the combination of the first three velocity channels presented in Figs. 3 and 4.

In the last velocity channel, $6.2 - 6.6$ kms^{-1}, emission comes primarily from the western side of the map. This component probably reaches its maximum beyond the western boundary of the map towards the core HCL2-A, which has an average velocity of 6.3 kms^{-1} (Cernicharo & Guélin 1987). In this velocity range the intensities of the 1665 and 1667 MHz lines are almost equal, which indicates a very high optical thickness. The overall velocity gradient apparent in the channel maps has been discussed by Schloerb & Snell (1984).

3.2. Excitation temperatures of the main lines and the column densities

The presence of heavily blended velocity components makes it difficult to derive reliably the optical thicknesses and excitation temperatures from the observed lines from the TMC-1 ridge. This is true even for the spectra with the highest signal-to-noise ratio shown in Fig. 1. Furthermore, the 'satellites' at 1612 and 1720 MHz exhibit anomaly in the sense that the 1612 is 'too strong' with respect to the main lines and the 1720. There is, however, no sign of 'main line anomalies' (cf. Crutcher 1979)

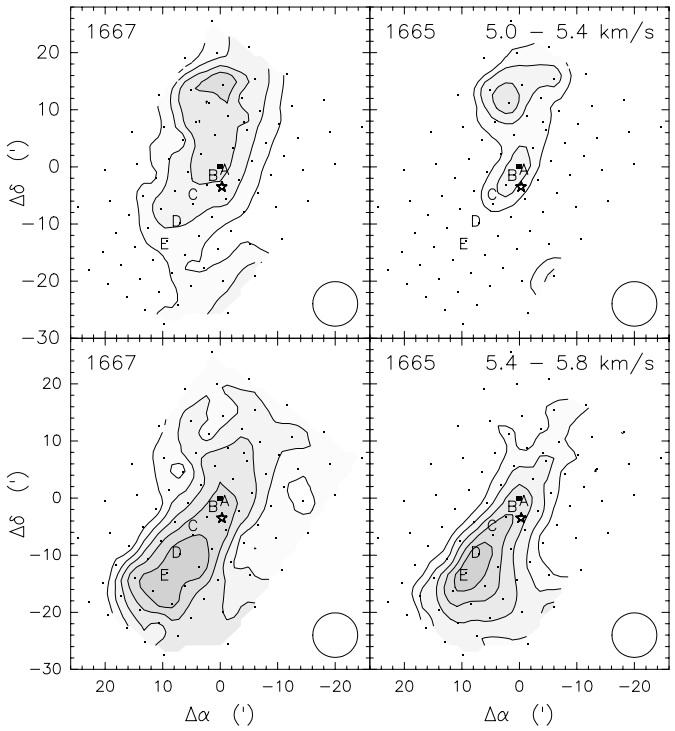

Fig. 3. Integrated intensity maps of the OH 1667 MHz (left) and 1665 MHz (right) lines in the velocity ranges $5.0-5.4$ and $5.4-5.8$ kms^{-1}. The lowest contour is 0.2 K kms^{-1} and the increments are 0.1 and 0.05 K kms^{-1} for the 1667 and 1665 MHz maps, respectively. The $(0,0)$ position and the location of IRAS 04381+2540 (39) are indicated. Also indicated are the locations of the dense cores, (A, B, C, D and E) as identified by Hirahara et al. (1992). The core D corresponds to the cyanopolyyne maximum, and core B corresponds to the ammonia maximum.

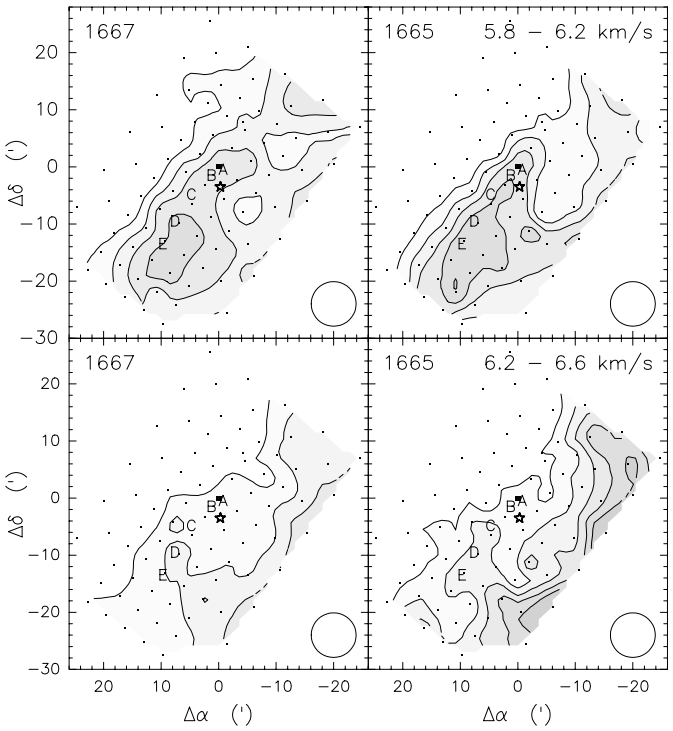

Fig. 4. Same as Fig. 3 but for the velocity ranges $5.8-6.2$ and $6.2-6.6$ kms^{-1}.

Table 1. Hyperfine structure fits to the 18-cm OH lines towards selected locations in TMC-1. For $(0',0')$ ($C^{18}O$ maximum) the fit is made to all four components, but for $(7\farcm0, 9\farcm8)$ ($12'$ southeast of $(0',0')$) only the main lines are used. The emitting gas is assumed to have two radial velocity components with gaussian distributions and the hyperfine components are assumed to have similar excitation temperatures.

$\Delta\alpha$ (′)	$\Delta\delta$	$v_{\rm LSR}$ (kms^{-1})	Δv (kms^{-1})	$T_{\rm MB}(1665)$ (K)	$\tau(1665)$	$T_{\rm ex}$ (K)
0	0	5.33(0.14)	0.37(0.47)	0.50(0.05)	0.46(0.10)	7.3*
		5.88(0.14)	1.17(0.47)	0.77(0.05)	0.55(0.10)	8.8*
7.0	-9.8	5.65(0.03)	0.24(0.03)	0.39(0.07)	0.20(0.02)	9.9*
		5.92(0.03)	1.24(0.04)	0.94(0.07)	0.88(0.02)	8.1*

* assuming that $\eta_c = 0.3$

towards TMC-1. Possible reasons for the observed anomaly are discussed in Sect. 4. Gaussian fits were made to the hyperfine structure of the spectra towards $(0',0')$ and $(7\farcm0, 9\farcm8)$. It was assumed that the emitting gas has two velocity components, and that the central velocities and the velocity dispersions of these components are similar for each hyperfine line. The results are presented in Table 1.

The excitation temperature, $T_{\rm ex}$, is derived from the main-beam brightness temperature, $T_{\rm MB}$, by assuming that the beam-source coupling efficiency, η_c, is 0.3. The adopted value is based on the impression from the total integrated intensity map presented in Fig 2. The dense ridge almost fills the circle representing the FWHM of the main beam, which would imply a beam-source coupling efficiency better than 0.25. It is furthermore assumed that the distributions of the OH main lines are relatively smooth, so that there is not much structure within the beam. The resulting values of $T_{\rm ex}$ are reasonable since low-level transitions of OH should be thermalized at densities typical of dense dark clouds (Rogers & Barret 1968; Guibert et al. 1978), and the kinetic temperature in TMC-1 is estimated to be about 10 K (e.g. Pratap et al. 1997).

The velocity component which corresponds to the TMC-1 ridge has a narrow line width, in consistence with previous measurements in other molecules. The value is, however, very uncertain due to overlap with the second velocity component. The peak optical thickness of the 1665 MHz line is moderate, i.e. ~ 0.5 towards $(0,0)$. As can be seen already from the relative intensities in Fig. 1 the optical thickness is lower and the excitation temperature is higher towards the cyanopolyyne maximum.

The results listed in Table 1 imply that the integrated intensity of the 1665 MHz line may be used for determining the column density assuming optically thin emission. The variation in the excitation temperature does not affect the derived column densities much as long as the values of $T_{\rm ex}$ stay well above the cosmic background temperature. The use of the 1667 MHz

line in a similar manner would lead to an underestimate of the column density.

The column density of OH, $N(\mathrm{OH})$, as a function of the integrated intensity of the 1665 MHz line (assuming that it is optically thin) is given by

$$N(\mathrm{OH})\,[\mathrm{cm}^{-2}] \;=\; 4.04\,10^{14}\frac{1}{1-T_{\mathrm{bg}}/T_{\mathrm{ex}}} \cdot\frac{1}{\eta_c}\int T_{\mathrm{MB}}(1665)dv\;[\mathrm{Kkms}^{-1}] \qquad (4)$$

(Turner 1966; Goss 1968).

The integrated 1665 MHz line intensity between 5.0 and 7.0 kms^{-1} is about 1.4 K km s^{-1} towards the offset $(7\farcm0, -9\farcm8)$ and several neighbouring locations in the southeastern part of the TMC-1 ridge. Assuming that $\eta_c = 0.3$ and $T_{\mathrm{ex}} = 10$ K (see above) one can derive there a total column density of $2.6\,10^{15}$ cm^{-2} for OH. In the velocity range where cyanopolyynes are detected, i.e. $5.4 - 6.2$ km s^{-1}, the column density is $1.5\,10^{15}$ cm^{-2}.

3.3. Comparison with other molecules

The integrated intensity map of the 1665 MHz OH emission resembles the C^{18}O($J = 1 - 0$) map obtained with the AT&T Bell Laboratories 7-m antenna (Langer et al. 1995, Fig. 1(a)), despite the different beamsizes available during the two observations. The beamsize of the 7-m antenna is $1\farcm7$ at 110 GHz. The main difference between the two maps is that the C^{18}O integrated intensity maximum lies towards our $(0, 0)$, whereas for OH this is located in the southeastern part of the ridge. The C^{18}O distribution in the map of Langer et al. (1995) is, however, relatively flat. The integrated C^{18}O($J = 1-0$) line intensity all over towards the dense ridge is ~ 2 K km s^{-1}, implying a C^{18}O column density of about $2\,10^{15}$ cm^{-2} or more depending on the beam-filling factor. Pratap et al (1997) derived C^{18}O column densities of about $3.5\,10^{15}$ cm^{-2} in the neighbourhood of our $(0, 0)$ and $(7\farcm0, -9\farcm8)$ positions. The latter observations were made with the 14-m FCRAO antenna (HPBW $\sim 50''$ at 110 GHz).

The fact that the OH and C^{18}O integrated intensity maxima lie in different places suggests that the column density ratio OH/C^{18}O varies along the ridge. In the following we examine this possibility with the aid of the C^{18}O data from Pratap et al. (1997).[1]

The derived OH column densities along the TMC-1 ridge increase gradually from the northwest to the southeast until reaching a maximum between the cyanopolyyne peak ($12'$ southeast of our $(0, 0)$) and the offset $(9\farcm3, -13\farcm0)$ ($16'$ southeast of $(0, 0)$). This is evident in Fig. 5, where we have plotted the OH column density along the cloud axis in the velocity range $5.4 - 6.2$ km s^{-1}, which is characteristic of the dense ridge. In Fig. 5 we have also indicated the C^{18}O column densities in the same velocity range derived from the data of Pratap et al. (1997). For this diagram we have used the data points lying closest to the cloud axis as defined in the present study. The solid line represents the averages of 9 pixels (sets of 3 by 3 pixels centered on the axis; the pixel size corresponds to the HPBW). The dotted line represents a map convolved to correspond to observations made with a $7\farcm8$ Gaussian beam.

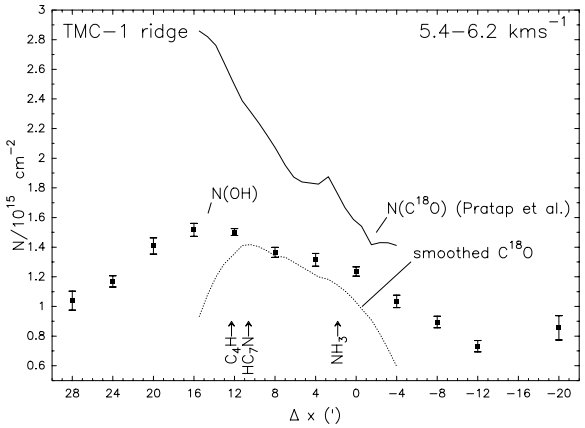

Fig. 5. The OH (square markers) and C^{18}O (dotted line) column densities along the TMC-1 ridge (i.e. along an axis going through our $(0, 0)$ and tilted by $54\fdg5$). The C^{18}O data is from Pratap et al. (1997) and interpolated to the indicated positions.

The C^{18}O integrated intensities between 5.4 and 6.2 km s^{-1} indicate a substantial column density gradient along the TMC-1 ridge. The decrease towards the ends of the curve representing the convolved data is due to the convolution routine which assumes zero intensity outside the map. Nevertheless, both curves show that the C^{18}O column density in this narrow radial velocity range increases towards southeast. The conclusion is that the column density ratio OH/C^{18}O does not increase from the ammonia peak to the cyanopolyyne maximum. The smoothed C^{18}O data indicates that the column density ratio $N(\mathrm{OH})/N(\mathrm{C}^{18}\mathrm{O})$ is ~ 1.

The channel maps in Figs. 3 and 4 can be compared with the C^{18}O, CS, SO, CCS and NH_3 maps from the same or roughly the same velocity ranges presented in Pratap et al. (1997, Figs. 2a-2c) and Hirahara et al. (1992, Figs. 4 and 8). Besides what is said above about C^{18}O, the comparison results in the following findings:

1) The CS($J = 2 - 1$) emission from the range $5.4 - 6.2$ kms^{-1} peaks in the northwestern part (Pratap et al. 1997, Fig. 2a) whereas the OH maximum in the same velocity range lies in the southeast.

2) The OH distribution bears no resemblance to the SO($J_N = 3_2 - 2_1$) map, except perhaps in the lowest velocity range $5.0 - 5.4$ kms^{-1}. In the next two channels, the OH peak moves to the southeast, whereas the SO peak remains in the northwest. The same is true also for the $NH_3(J, K = 1, 1)$ distribution (Hirahara et al. 1992, Fig. 8).

3) The OH distribution in the range $5.4 - 6.2$ kms^{-1} agrees well with the CCS($J_N = 4_3 - 3_2$) distribution (Hirahara et al. 1992, Fig. 4). The CCS emission correlates well with HC_3N and other cyanopolyynes, which peak towards the Hirahara clump D (Hirahara et al. 1992, Fig. 4).

[1] available via the NCSA Astronomy Digital Image Library (ADIL)

It should be noted that in the diagrams in Figs. 12 and 13 of Pratap et al. (1997), where column density ratios and volume densities are presented as a function of angular distance measured along the ridge from their $(0,0)$ positions, our $(0,0)$ correponds roughly to the offset $-8'$, and our $(7'.0, -9'.8)$ corresponds to the offset $+4'$. From Fig. 13 of Pratap et al. (1997) it can be seen that the OH maximum is coincident with the location where the number density of H_2 starts to drop.

4. Discussion

4.1. Comparison with chemistry models

In the previous section it was found that the column density ratio $N(\mathrm{OH})/N(\mathrm{C^{18}O})$ is about unity in the dense ridge of TMC-1. Using the relation between the $C^{18}O$ column density and the visual exctinction (which can be converted to the total H_2 column density) deduced by Frerking et al. (1982) towards dense cores in Taurus, one obtains for OH a fractional abundance of $\sim 1.5\,10^{-7}$. This is in agreement with the earlier result presented in Irvine et al. (1985). The relation between $N(\mathrm{C^{18}O})$ and $N(\mathrm{H_2})$ was derived for the visual extiction range $4 \leq A_V < 21$. The recent results of Caselli et al. (1999) indicate that CO can be depleted by a factor of ten due to freezing onto the grain surfaces in the centres of dense cores, and that the use of a constant value for the fractional CO abundance is not always justified. However, the depletion of CO becomes significant in regions with the densities above 10^5 cm^{-3} (Caselli et al. 1999) which form only a small fraction of the gas traced by the $C^{18}O$ and OH observations discussed here (Pratap et al. 1997). Therefore we infer that the derived fractional OH abundance must be correct to the order of magnitude.

The high fractional abundance of OH ($\sim 10^{-7}$) in dense gas implies that electronic recombination of H_3O^+ produces effectively OH besides H_2O, and is therefore consistent with the 'old' picture of dissociative recombination put forth by Green & Herbst (1979) and the experimental results of Vejby-Christensen et al. (1997). As discussed in Millar et al. (1988) and Millar (1990) the fractional OH abundance would be two orders of magnitude lower ($\sim 10^{-9}$) in case it would not be formed in the recombination of H_3O^+.

Keeping to the production of OH by electronic recombination, we discuss the finding that its distribution in TMC-1 correlates well with those of CCS and and cyanopolyynes, but is very different from the SO and NH_3 distributions. Chemistry models predict the following dependence of the fractional OH abundance on physical conditions and time:

1) The fractional OH abundance depends on the gas density via the formation of H_3^+. It should be *larger* at lower densities (e.g. Viala 1986; Lee et al. 1996).

2) Recent time-dependent pure gas-phase chemistry models of dense clouds predict an increase in the fractional OH abundance with time, which reflects the decrease in the atomic O abundance (Lee et al. 1996; Millar et al. 1997), whereas earlier results indicated a tendency to decrease with time because of conversion to O_2 (e.g. Brown & Rice 1986). This is due to the fact that formerly a higher rate coefficient for reaction (2) was used (Millar et al. 1997). Nevertheless, the time dependence of OH is rather weak, compared for example with what is predicted for O_2, HC_3N or C_4H (Lee et al. 1996; Millar et al. 1997; Ruffle et al. 1997). Therefore OH is not particularly good as an age indicator, as far as only gas-phase reactions are considered.

3) Accretion of neutral species on to grain surfaces affects the fractional abundance of OH. Firstly, depletion reduces the destruction of H_3^+ via reducing the abundance of neutral atoms and molecules in the gas phase (Viala 1986; Brown & Millar 1989). The enhancement of H_3^+ compensates the diminished supply of atomic O, and the production of OH remains nearly unchanged (Viala 1986). At the same time its destruction rate via reaction (2) is reduced. Therefore depletion tends to *increase* the fractional abundance of OH. The same is happening to other radicals. This increase of radicals is coincident with the enhancement of deuterated species (Brown & Millar 1989).

The gas density in the TMC-1 ridge, as derived in Pratap et al. (1997, see their Figs. 9 and 13), is almost constant, increasing at most by a factor of 2.5 from the cyanopolyyne peak to the ammonia peak, whereas in Hirahara et al. (1992) the estimated gradient is steeper, corresponding to an increase by one order of magnitude over the same distance. Pratap et al. used for their density determination three transitions of HC_3N which they observed with almost similar beams of $\sim 1'$, whereas Hirahara observed two transitions of $C^{34}S$ with beamsizes of $34''$ and $17''$. The discrepancy between the results is probably due to the different angular resolutions and the fact the Hirahara et al. (1992) did not correct for different beamsizes at the two frequencies used, i.e. they assumed an extended uniform source. The density structure determined by Pratap et al. (1997) is consistent with little variation in the fractional OH abundance, whereas the results of Hirahara et al. would imply a clearly higher abundance of OH in the southeastern part of the cloud and therefore do not quite fit the present observations.

The cyanopolyyne peak in the southeastern part of the cloud has been claimed to represent an earlier stage of chemical evolution than does the northwestern part (e.g. Suzuki et al. 1992; Hirahara et al. 1992; Howe et al. 1996). Carbon-chain molecules are produced efficiently in the gas phase when the abundance of neutral C or C^+ is large, which is considered to be the case before steady state is reached (Leung et al. 1984; Herbst & Leung 1989). On the other hand, the fact that both NH_3 and N_2H^+ peak at the northwestern end suggests an advanced stage since the formation of these molecules involves N_2, the abundance of which is mainly controlled by slow neutral-neutral reactions (e.g. Suzuki et al. 1992; Hirahara et al. 1992). Chemical evolution could provide an explanation also for the higher SO abundance at the northwestern end, because SO is formed in the neutral-neutral reactions and destroyed by neutral carbon (Hirahara et al. 1995; Nilsson et al. 2000). As discussed above, lapse of time and an increase in density lead the fractional OH

abundance in contrary directions, but the evolutionary effect is probably much weaker.

According to the results of Ruffle et al. (1997), a high abundance of complex carbon compounds may also be associated with efficient accretion onto dust grain surfaces, which besides leads to an enhanced formation of CH and OH (Brown & Millar 1989). Against this background it is intriguing that the OH, CCS and HC_3N distributions peak in the same part of the cloud. Moreover, the recent pure gas-phase chemistry models of Nilsson et al. (2000) predict that for a fixed C/O ratio the SO/CS abundance ratio increases with time. The SO and CS maps of TMC-1 obtained by Pratap et al. (1997, Figs. 1, 2a and 2c) are, however, fairly similar, both peaking near the ammonia maximum. These results raise a doubt about the chemical age difference hypothesis and seem to lend support to the alternative that the abundance variations in TMC-1 depend on the differences in the degree of depletion. As discussed in Hartquist et al. (1996), the lower degree of depletion in the denser northwestern part could be understood by more efficient desorption in the vicinity of IRAS 04381+2540.

The difficulty in the depletion model is that it should also explain the lower abundances of CS, SO, NH_3, N_2H^+ etc. observed in the southeastern part of TMC-1. The effect of the gas-grain surface interaction on the abundances of simple molecules in prestellar cores have been modelled by Bergin & Langer (1997). In these time-dependend models it turns out that CS and SO can indeed deplete at very late stages of chemical evolution. (This phase is preceded by a prominent maximum in the SO abundance.) By this time also CCS should have almost disappeared from the gas phase, which however does not correspond to the situation observed in TMC-1. As to CO, in the model of Ruffle et al. (1997) the fractional abundance of CO should have decreased by a factor of about ten during the second cyanopolyyne peak, but according to Bergin & Langer (1997) this depends heavily on the grain mantle composition. On the other hand, N_2H^+ and NH_3 do not deplete for any mantle composition and should by all likelyhood have high abundances also in the southeastern part of TMC-1.

Thus it seems that the abundance variations and in particular the cyanopolyyne peak in TMC-1 cannot be explained by depletion. For the gas-phase time dependent models the agreement is considerably better, but not perfect (cf. the SO/CS ratio). The coming observations with Odin of the 119 GHz ground state transition of O_2 may provide the final solution of this issue. If the SO maximum in the northwestern end of TMC-1 indeed represents later stages of chemical evolution, one would expect that also the O_2 abundance reaches its maximum towards this location. The slightly lower column density of OH in the northwestern part would be due to its conversion to O_2 and SO, and at later stages these molecules can remain in the gas phase due to a low abundance of carbon atoms (Millar & Nejad 1985; Millar & Herbst 1990; Nilsson et al. 2000). On the other hand, if accretion on to grains determines the chemical composition, the O_2 maximum is expected to be found towards the cyanopolyyne peak (Willacy & Williams 1993).

4.2. Satellite anomalies

Enhanced 1612 MHz emission observed towards TMC-1 represents an anomaly found also in circumstellar envelopes and is referred to as type II(b) (Turner 1973). The dark cloud 2D of Turner (1973) observed with the NRAO 43-m telescope lies adjacent to the dense ridge corresponding to the offset $(7'.0, -6'.3)$ from our $(0, 0)$. According to him the two velocity components seen in the spectrum, 5.6 and $\sim$ 6.8 km s^{-1}, represent type II(b) and II(a) (1720 enhanced) anomalies, respectively. As can be seen in Fig. 1, in our observations towards two neighbouring locations both velocity components exhibit type II(b) anomaly. Also gaussian fits to the hyperfine structure, which persistenly divide the lines into a narrow, lower velocity and broad, higher velocity components, give the same result. The controversy with the result of Turner (1973) probably can be attributed to the different angular and spectral resolutions used.

Enhanced 1612 MHz emission is caused by an overpopulation of the $F = 1$ sublevels of the ground state $^2\Pi_{3/2}(J = 3/2)$ of OH with respect to those of $F = 2$. Due to this overpopulation the excitation temperature, $T_{\rm ex}$, of the 1612 MHz transition ($F = 1 \rightarrow 2$) is higher, and the $T_{\rm ex}$ of the 1720 MHz line ($F = 2 \rightarrow 1$) is lower than that of the main lines ($F = 2 \rightarrow 2$ and $F = 1 \rightarrow 1$). Note that the excitation temperatures of the four transitions are bound by a sum rule resulting from the Boltzmann equation (e.g. Crutcher 1977), so that if the main lines are in LTE and $T_{\rm ex}(1612)$ is higher than the equilibrium value, $T_{\rm ex}(1720)$ must be lower than that.

Overpopulation of the ground levels with $F = 1$ can arise when the molecules cascade down, after having been pumped in some way into higher levels, via the transition $^2\Pi_{1/2}(J = 1/2) \rightarrow {}^2\Pi_{3/2}(J = 3/2)$ (cf. Elitzur 1976). The state $^2\Pi_{1/2}(J = 1/2)$ involved in the generation of enhanced 1612 MHz emission is the third lowest one and has an energy of about 180 K. Excitation of this state in an otherwise cool cloud can be best explained by radiative pumping at wavelengths shortwards of $\lambda = 80\mu$m (Litvak 1969; Turner 1973; Elitzur 1976).

Another way to produce overpopulation of the $F = 1$ level according to Crutcher (1977) is self-shielding by the optically thick $F = 1 \rightarrow 2$ transitions between the ground state and the $^2\Pi_{3/2}(J = 5/2)$ state in the presence of a nearby infrared source radiating at 120 μm. The $F = 2$ levels of the ground state would be drained via absorption of the far-infrared radiation by the optically thin $F = 2 \rightarrow 2$ transitions to the upper level.

The mapped region contains at least one embedded young stellar object (YSO) and is surrounded by several others (see Figs. 2 – 3; Onishi et al. 1998). The embedded YSO near the map centre is IRAS 04381+2540 labelled by 39 (referring to Table 3 in Onishi et al. 1998). This source is also associated with a compact outflow and a near-infrared nebulosity (Moriarty-Schieven et al. 1992).

The unlabelled source north of IRAS 04381+2540 is IRAS 04380+2553 (marked with a cross), an optically visible star with a far-infared spectrum rising steadily from 12 to 100 μm. This source may lie on the fringes of the cloud with the far-infrared

radiation coming from the surrounding dust. The unlabelled source in the southern part of the map is IRAS 04383+2527, which was detected only in the 100μm band, and possibly is a cirrus knot.

The labelled objects near the borders of the map (37: IRAS 04368+2557, 38: IRAS 04369+2539, 41: IRAS 04390+2517) are according to Onishi et al. (1998) YSO's embedded in the cloud. There are two more embedded sources (IRAS 04361+2547 and IRAS 04365+2535) beyond the western boundary of the map. All these objects are central sources of localized outflows (Heyer et al. 1987; Moriarty-Schieven et al. 1992). IRAS 04369+2539 is furthermore associated with a tiny optical reflection nebula (IC 2087).

Besides the point sources, the cloud exhibits extended emission in the 60 and 100 μm bands of IRAS Sky Survey (Wheelock et al. 1994[2]). The extended far-infrared emission peaks towards IRAS 04383+2527 (the suspected cirrus source) in the south but continues also further south beyond the map.

The satellite line ratios have been measured only in two locations, one close to IRAS 04381+2540, the other about $12'$ off towards the cyanopolyyne maximum, which has no infrared sources in its vicinity. However, in both directions the anomaly is similar. Therefore it is likely that the enhanced 1612 MHz line emission is not localized to the immediate surroundings of IRAS point sources. The required extended far-infrared radiation field probably originates from heated dust, but may also come from the OH itself in terms of fluorescence from rotational states following the excitation of vibrational levels by near-infrared emission from the point sources (Litvak 1969). The average central velocity of the CO outflows associated with the IRAS sources is 6.4 kms^{-1} (Heyer et al. 1987; Moriarty-Schieven et al. 1992). Therefore most of these sources are likely to be enshrouded by the extended, higher velocity cloud component. A mapping in the 1612 MHz and 1720 MHz satellite lines would probably yield more decisive information of the rôle of embedded infrared souces in the OH excitation.

5. Conclusions

The OH distribution in the TMC-1 ridge is similar to those of CCS and HC_3N, peaking towards the cyanopolyyne maximum, and different from SO and NH_3 which reach their maxima towards the northwestern part of TMC-1. The OH/$C^{18}O$ column density ratio, and probably also the fractional OH abundance remain, however, almost constant throughout the dense ridge. The fractional OH abundance there is of the order 10^{-7}. This high value confirms that OH is efficiently formed by dissociative electron recombination of H_3O^+.

The fact that the OH abundance does not change much along the TMC-1 ridge is in agreement with the relatively flat density distribution derived by Pratap et al. (1997). If the gas density and other physical characteristics are indeed similar towards the ammonia and cyanopolyyne maxima it is natural to seek for an explanation to their chemical differences in chemical evolution (e.g Suzuki et al. 1992) and in effects of freezing-out of neutral species on to grain surfaces (Ruffle et al. 1997).

The SO and CS mapping results of Pratap et al. (1997) together with the recent chemistry model results of Nilsson et al. (2000) seem to be in conflict with the idea that the ammonia peak is chemically more mature than the cyanopolyyne peak. Moreover, the similarity of the OH and HC_3N distributions as such could be understood by a higher degree of depletion towards the cyanopolyyne peak. However, the relative distributions of several other molecules (e.g. CCS, N_2H^+ and NH_3) do not fit the latter model (Bergin & Langer 1997). Therefore the observed chemical gradient in TMC-1 is most likely produced by time-dependend gas-phase reactions after all. The possible detection of O_2 towards either the ammonia or the cyanopolyyne peak would be a crucial test between the freezing-out and gas-phase evolution models.

The OH lines exhibit a satellite line anomaly, where the 1612 MHz line is stronger and the 1720 MHz line is weaker than expected from the main line intensities under LTE assumption. The most probable explanation for the anomalous excitation is far-infrared continuum emission from dust heated by the young stellar objects embedded in the cloud.

Acknowledgements. We thank Dr. A. Heikkilä for helpful discussions and the referee, Dr. T.J. Millar, and Professors J.H. Black and Å. Hjalmarson for very useful comments on the manuscript. The work by J.H. was supported by the Academy of Finland through grant No. 1011055. J.G.A.W. acknowledges support from the Deutsche Forschungsgemeinschaft through grant SFB-301. The authors would like to thank Dr. P. Pratap and the NCSA Astronomy Digital Image Library (ADIL) for providing the $C^{18}O$ data of TMC-1 for this article.

[2] examined with the SkyView Virtual Observatory (http://skview.gsfc.nasa.gov), which is developed at the GSFC Laboratory for High Energy Astrophysics of NASA

References

Bergin E.A., Langer W.D., 1997, ApJ 486, 316
Bergman P., 1995, ApJ 445, L167
Brown P.D., Millar T.J., 1989, MNRAS 237, 661
Brown R.D., Rice E.H.N., 1986, MNRAS 223, 405
Caselli P., Walmsley C.M., Tafalla M., Dore L., Myers P.C., 1999, ApJ 523, L165
Cernicharo J., Guélin M., 1987, A&A 176, 299
Cernicharo J., Guélin M., Askne J., 1984, A&A 138, 371
Churchwell E., Winnewisser G., Walmsley C.M., 1979, A&A 67, 139
Crutcher R.M., 1977, ApJ 216, 308
Crutcher R.M., 1979, ApJ 234, 881
Elitzur M., 1976, ApJ 203, 124
Frerking M.A., Langer W.D., Wilson R.W., 1982, ApJ 262, 590
Goss W.M., 1968, ApJS 15, 131
Green S., Herbst E., 1979, ApJ 229, 121
Guélin M., Langer W.D., Wilson R.W., 1982, A&A 107, 107
Guibert J., Elitzur M., Nguyen-Q-Rieu, 1978, A&A 66, 395
Hartquist T.W., Williams D.A., 1995, The chemically controlled cosmos. Cambridge University Press, p. 58
Hartquist T.W., Williams D.A., Caselli P., 1996, Ap&SS 238, 303
Herbst E., 1983, ApJS 53, 41
Herbst E., Leung C.M., 1989, ApJS 69, 271
Heyer M.H., Snell R.L., Goldsmith P.F., Myers P.C., 1987, ApJ 321, 370

Hirahara Y., Suzuki H., Yamamoto S., et al., 1992, ApJ 394, 539
Hirahara Y., Masuda A., Kawaguchi K., et al., 1995, PASJ 47, 1
Howe D.A., Taylor S.D., Williams D.A., 1996, MNRAS 279, 143
Irvine W.M., Schloerb F.P., Hjalmarson Å., Herbst E., 1985, In: Black D.C., Matthews M.S. (eds.) Protostars & Planets II, Arizona University Press, Tucson, p. 579
Langer W.D., Velusamy T., Kuiper T.B.H., et al., 1995, ApJ 453, 293
Lee H.-H., Bettens R.P.A., Herbst E., 1996, A&AS 119, 111
Leung C.M., Herbst E., Huebner W.F., 1984, ApJS 56, 231
Little L.T., MacDonald G.H., Riley P.W., Matheson D.N., 1979, MNRAS 189, 539
Litvak M.M., 1969, ApJ 156, 471
Maréchal P., Viala Y.P., Benayoun J.J., 1997, A&A 324, 221
Millar T.J., 1990, In: Hartquist T.W. (ed.) Molecular Astrophysics - A Volume Honouring Alex Dalgarno. Cambridge University Press, p. 115
Millar T.J., Herbst E., 1990, A&A 231, 466
Millar T.J., Nejad L.A.M., 1985, MNRAS 217, 507
Millar T.J., DeFrees D.J., McLean A.D., Herbst E., 1988, A&A 194, 250
Millar T.J., Farquhar P.R.A., Willacy K., 1997, A&AS 121, 139
Moriarty-Schieven G.H., Wannier P.G., Tamura M., Keene J., 1992, ApJ 400, 260
Nilsson A., Hjalmarson Å., Bergman P., Millar T.J., 2000, A&A, in press
Olano C.A., Walmsley C.M., Wilson T.L., 1988, A&A 196, 194
Onishi T., Mizuno A., Kawamura A., Ogawa H., Fukui Y., 1998, ApJ 502, 296
Ott M., Witzel A., Quirrenbach A., et al., 1994, A&A 284, 331
Phillips T.R., Green S., 1995, Ap&SS 224, 537
Pratap P., Dickens J.E., Snell R.L., et al., 1997, ApJ 486, 862
Rogers A.E.E., Barrett A.H., 1968, ApJ 151, 163
Ruffle D.P., Hartquist T.W., Taylor S.D., Williams D.A., 1997, MNRAS 291, 235
Schloerb F.P., Snell R.L., 1984, ApJ 283, 129
Suzuki H., Yamamoto S., Ohishi M., et al., 1992, ApJ 392, 551
Takakuwa S., Mikami H., Saito M., 1998, ApJ 501, 723
Turner B.E., 1966, Nat 212, 184
Turner B.E., 1973, ApJ 186, 357
Vejby-Christensen L., Andersen L.H., Heber O., et al., 1997, ApJ 483, 531
Viala Y.P., 1986, A&AS 64, 391
Wheelock S.L., Gautier T.N., Chillemi J., et al, 1994, IRAS sky survey atlas: Explanatory supplement. Publication of the National Space Flight Data Center
Willacy K., Williams D.A., 1993, MNRAS 260, 635

Note added in proof: Professor Å. Hjalmarson pointed out that in fact the $C^{34}S$ and SO maps or Pratap et al. (1997) shown in their fig. 10 conform with the predictions of Nilsson et al. (2000) and the main conclusion from the present study. Professor J.H. Black remarked that the extended far-infrared radiation field, even if it is only slightly more intense than the general Galactic background in the solar neighbourhood, can efficiently excite the rotational states of OH. Thus the vicinity of IR point sources is not necessarily needed to explain the satellite anomalies of the 18-cm OH lines.